

## On the energy conversion efficiency in magnetic hyperthermia applications: A new perspective to analyze the departure from the linear regime

G. T. Landi and A. F. Bakuzis

Citation: *J. Appl. Phys.* **111**, 083915 (2012); doi: 10.1063/1.4705392

View online: <http://dx.doi.org/10.1063/1.4705392>

View Table of Contents: <http://jap.aip.org/resource/1/JAPIAU/v111/i8>

Published by the [American Institute of Physics](#).

---

### Related Articles

Fabrication of glycerol liquid droplet array by nano-inkjet printing method

*J. Appl. Phys.* **111**, 074319 (2012)

A controlled biochemical release device with embedded nanofluidic channels

*Appl. Phys. Lett.* **100**, 153510 (2012)

Effects of DNA nucleotide adsorption on the conductance of graphene nanoribbons from first principles

*Appl. Phys. Lett.* **100**, 153117 (2012)

Fe<sub>3</sub>O<sub>4</sub>-citrate-curcumin: Promising conjugates for superoxide scavenging, tumor suppression and cancer hyperthermia

*J. Appl. Phys.* **111**, 064702 (2012)

Integrated intravital microscopy and mathematical modeling to optimize nanotherapeutics delivery to tumors

*AIP Advances* **2**, 011208 (2012)

---

### Additional information on *J. Appl. Phys.*

Journal Homepage: <http://jap.aip.org/>

Journal Information: [http://jap.aip.org/about/about\\_the\\_journal](http://jap.aip.org/about/about_the_journal)

Top downloads: [http://jap.aip.org/features/most\\_downloaded](http://jap.aip.org/features/most_downloaded)

Information for Authors: <http://jap.aip.org/authors>

## ADVERTISEMENT



Special Topic Section:  
**PHYSICS OF CANCER**

Why cancer? Why physics? [View Articles Now](#)

# On the energy conversion efficiency in magnetic hyperthermia applications: A new perspective to analyze the departure from the linear regime

G. T. Landi<sup>1,a)</sup> and A. F. Bakuzis<sup>2</sup>

<sup>1</sup>*Instituto de Física da Universidade de São Paulo, 05314-970 São Paulo, Brazil*

<sup>2</sup>*Universidade Federal de Goiás, Instituto de Física, 74001-970, Goiânia-GO, Brazil*

(Received 11 January 2012; accepted 21 March 2012; published online 26 April 2012)

The success of magnetic hyperthermia cancer treatments rely strongly on the magnetic properties of the nanoparticles and their intricate dependence on the externally applied field. This is particularly more so as the response departs from the low field linear regime. In this paper we introduce a new parameter, referred to as the efficiency in converting electromagnetic energy into thermal energy, which is shown to be remarkably useful in the analysis of the system response, especially when the power loss is investigated as a function of the applied field amplitude. Using numerical simulations of dynamic hysteresis, through the stochastic Landau-Lifshitz model, we map in detail the efficiency as a function of all relevant parameters of the system and compare the results with simple—yet powerful—predictions based on heuristic arguments about the relaxation time. © 2012 American Institute of Physics. [<http://dx.doi.org/10.1063/1.4705392>]

## I. INTRODUCTION

Magnetic hyperthermia is a rapidly developing technique in medical research and oncology.<sup>1–4</sup> It is based on the dissipation in the form of heat caused by magnetic nanoparticles under the influence of a high-frequency external magnetic field  $\mathbf{H}(t) = \mathbf{H}_0 \cos \omega t$ . Considerable effort has been made to optimize the materials properties for this application. From the chemical standpoint, for instance, it is necessary to adequately functionalize the particle's surface with molecules that selectively adhere to cancerous cells, thus leaving healthy cells unharmed. As for the magnetic properties of the particles, one aims at maximizing the power dissipated per unit mass—called the specific absorption rate (SAR). This is also subject to biological restrictions, such as avoiding toxic materials or using sufficiently low frequencies and field amplitudes to prevent the formation of eddy currents inside the patient's body. Because of these issues, several papers have focused on ferrite-based nanostructures,<sup>5–12</sup> in particular, magnetite-coated nanoparticles, which have already been approved by the FDA for diagnosis purposes, such as contrast agents in magnetic resonance imaging.<sup>13</sup>

The fundamental concept underlying magnetic hyperthermia concerns the dissipation mechanisms of the magnetization, a subject of intensive experimental<sup>3,14</sup> and theoretical research.<sup>1,15–20</sup> Historically, Gilchrist *et al.*,<sup>21</sup> which was the first to propose this application, had already pointed out to three distinct possibilities, namely, dielectric, eddy current, and hysteresis losses. The first two are believed to be irrelevant for ferrite-based nanoparticles, while the latter can be related to both domain wall motion in sufficiently large particles or (in) coherent spin rotation under alternating magnetic fields. Since the nanoparticles in this context are usually smaller than the critical single-domain size,<sup>22</sup> the contribution from domain walls may also be safely neglected. In this paper we thus consider only single-domain

nanoparticles and assume, for simplicity, that coherent rotation is the only relevant reversal mechanism. In this case the heat production may be directly associated with irreversible overbarrier jumps taking place between the stable energy minima formed by the anisotropy potential.<sup>23</sup> In addition, it is also necessary to take into account the intrinsic magnetization damping stemming from the interaction (via the spin-orbit coupling) of the individual spins with electronic degrees of freedom.<sup>16</sup> In any case, however, it is important to note that all dissipation mechanisms are actually entangled so that their relative contributions cannot be individually retrieved from experiment.

Experimentally, the SAR is usually computed from calorimetry experiments, being proportional to the initial slope of the heating rate curve. Conversely, the theoretical approach is to first simulate the hysteresis loop formed by plotting the projection of the magnetization onto the magnetic field [here denoted as  $M(t)$ ] vs.  $H(t)$ . This follows from the fact that magnetic hyperthermia belongs to the broader scope of dynamic hysteresis,<sup>1,17–20,24–26</sup> where one measures the magnetic response to an alternating magnetic field of arbitrary strength, frequency, and direction. Then, on noting that the magnetic work performed by the system is simply  $HdM$ , the first law of thermodynamics immediately implies that the energy dissipated per hysteresis cycle is precisely the area of the hysteresis loop ( $A$ ).<sup>27</sup> The SAR, in turn, is given simply by  $fA$ , where  $f = \omega/2\pi$  is the frequency of the magnetic field. That this approach in fact agrees with calorimetry measurements was recently demonstrated experimentally in Ref. 28.

A theoretical description of magnetic hyperthermia thus involves computations of dynamic hysteresis using some suitable model capable of accounting for the aforementioned damping mechanisms. For instance, in the present paper we employ the Néel-Brown theory,<sup>29,30</sup> corresponding to the stochastic version of the Landau-Lifshitz equation. This approach is both robust and flexible, enabling one to compute the response to any field amplitude or frequency with

<sup>a)</sup>Electronic mail: [glandi@gmail.com](mailto:glandi@gmail.com).

great accuracy. However, being an intrinsically non-linear problem, no analytical solutions are available, forcing one to resort exclusively to numerical calculations.

Alternatively, if the field amplitude  $H_0$  is sufficiently small, one expects that  $M(t) \propto H_0$ , corresponding to the linear response regime. Solution methods in this case also have the Néel-Brown theory as a starting point, which is then used in conjunction with the linear response theory.<sup>30</sup> Formally, even in this case, no closed form solutions exist. Notwithstanding, several approximate but accurate formulae have been developed.<sup>30–32</sup> Owing to the existence of such expressions, the linear regime has been in the center of much of the recent literature on magnetic hyperthermia. This is unfortunate given that, in the quest to optimize the heating capabilities of the material, the field amplitude directly determines the energy input, thence being a parameter of utmost importance. As a matter of fact, combining high anisotropy particles with sufficiently large fields may entail losses that are orders of magnitude larger than the linear response, while simultaneously remaining well within the aforementioned biological restrictions.

Except for some recent studies,<sup>1,18,33</sup> the transition between the linear and non-linear regimes has not yet been theoretically explored in detail within the context of single-domain particles. Most papers have focused either exclusively on the linear response theory<sup>15,32,34</sup> or on the other extreme of high field amplitudes.<sup>17,19,20,24–26</sup> For magnetic hyperthermia, the latter is not of much interest given that such high fields are both difficult to achieve in the laboratory and possibly hazardous to the patient. It is also known both experimentally<sup>3,35</sup> and theoretically<sup>30,33</sup> that the linear regime is in fact an asymptotic approximation to the limit of zero field amplitude so that even small fields should already manifest measurable nonlinearities. The question then follows as to whether or not these deviations contain interesting physical information about the system, which may enable one to better understand the damping mechanisms involved and, perhaps, even predict the system's response to even higher field amplitudes. As an example, it is well known that the heating rate shows a maximum depending on the physical parameters (diameter or anisotropy constant) of the material. The probing of such, however, may be quite challenging experimentally given the large number of samples necessary and the thorough knowledge of the structural and morphological properties of each that is required. In this paper we will show how it is possible to identify, via a field amplitude hyperthermia analysis, if the particles are at the high barrier or low barrier regime. This, in turn, can be used as a guideline to optimize the heating properties of the material.

It is the purpose of this paper to discuss in detail the magnetic response as the system departs from the linear regime. In Sec. II we review some relevant properties of the linear response theory and show how heuristic arguments may be employed to qualitatively predict this departure, yielding additional insight into the energy barrier distribution of the system. In Sec. III we briefly introduce the Néel-Brown theory, whose solution methods are described in the Appendix and which may be employed to compute dynamic hysteresis loops in any condition desired. Results of the

numerical calculations are presented in Sec. IV where the dependence of the SAR with the field amplitude is probed in detail. For clarity, these results concern mono-disperse particle assemblies, a restriction which is then lifted in Sec. V, where poly-disperse samples with a lognormal distribution are briefly discussed. Finally, Sec. VI provides the conclusions.

## II. LINEAR REGIME

In the linear regime the magnetization, albeit closely following the oscillating magnetic field, will do so with a phase lag. A parametric graph of  $M(t)$  vs.  $H(t)$  thus yields an ellipse, the area of which may be identified with the energy dissipated during each cycle,<sup>27</sup> as mentioned in Sec. I. If we write  $M(t) = H_0[\chi'(\omega) \cos \omega t - \chi''(\omega) \sin \omega t]$ , where  $\chi'$  and  $\chi''$  are the real and imaginary susceptibilities, then a simple computation shows that  $A_0 = \pi H_0^2 \chi''(\omega)$  (the subscript 0 indicates that the result is exclusive of the linear regime). It is the premise of the linear response theory that, through the fluctuation-dissipation theorem, one can relate the AC susceptibility to the relaxation properties of the system. In the event that the latter is dictated by a single relaxation time ( $\tau$ ), the susceptibility takes the form of the famous Debye factor,  $\chi''(\omega) = \chi_0 \omega \tau / (1 + (\omega \tau)^2)$ , where  $\chi_0$  is the static susceptibility (these concepts have a broader range of applicability and are discussed in detail in the books by Scaife<sup>36</sup> and Coffey *et al.*<sup>30</sup> For a discussion specific to single-domain particles or ferro-fluids, cf., Refs. 1 and 32.). Whence

$$A_0 = \pi H_0^2 \chi_0 \frac{\omega \tau}{1 + (\omega \tau)^2}. \quad (1)$$

This equation should be interpreted as an asymptotic expression for  $H_0 \rightarrow 0$  and is expected to hold as long as the field does not distort significantly the energy landscape of the particle. We restrict our discussion to Néel relaxation—where only the magnetization vector is allowed to rotate—and also assume a single effective uniaxial anisotropy. These are common assumptions, well justified from experimental grounds.<sup>37–39</sup> In this case an adequate expression for the relaxation time, assuming uniaxial anisotropy, is the Néel-Brown formula<sup>29</sup>

$$\tau = \tau_0 \sqrt{\frac{\pi}{\sigma}} e^{\sigma}, \quad (2)$$

where  $\sigma = Kv/k_B T$ ,  $K$  being the anisotropy constant (assumed uniaxial) and  $v$  the particle's volume. Equation (2) is valid for  $\sigma > 1$  and accurate to  $\sim 10\%$  with respect to the exact value, which may be computed, for instance, by the methods described in the Appendix. On noting that the magnetic properties of the particles are almost entirely dictated by  $\tau$ , which, in turn, depends exponentially on  $\sigma$ , it becomes clear that the latter is the most important parameter in this type of system. We also note that, except for a scaling constant, the static susceptibility is well described<sup>30</sup> by  $\chi_0 \sim \sigma - 1$ .

It is important to note that, within the present context, the area and the SAR are practically equivalent quantities

since most experiments are performed at a fixed frequency. In this paper we will frequently speak of  $A$ , and it is understood that the relation  $\text{SAR} = fA$  may be used to convert between one and the other.

Equation (1) predicts that initially  $A_0$  should increase quadratically with  $H_0$ . The central question, discussed in this paper, is how it will behave as the system departs from the linear regime. Intuitively, one expects it to be a monotonically increasing function, eventually saturating at sufficiently high fields. This type of behavior is not easily analyzed. See, for instance, Fig. 2(a) (to be properly discussed below): all curves rise quickly, crossing one another at different positions and saturating at different values. In other words, from an experimental viewpoint, plotting  $A$  (or the SAR) vs.  $H_0$  for different samples, yields little information on how the magnetic properties of the material affect its heating capabilities.

On the other hand, note that this quadratic dependence ( $A_0 \propto H_0^2$ ) actually incites an interesting physical interpretation since  $H_0^2$  is proportional to the electromagnetic energy density in the vicinity of the particles. Whence, we may define the *efficiency in converting electromagnetic energy into thermal energy* as

$$\Omega = \frac{A}{H_0^2}. \quad (3)$$

Thus, from Eq. (1) we see that the linear response efficiency ( $\Omega_0$ ) is independent of  $H_0$

$$\Omega_0 = \pi\chi_0 \frac{\omega\tau}{1 + (\omega\tau)^2}. \quad (4)$$

Equation (3) is plotted with a dashed line in Fig. 1, to be discussed below (it practically coincides with the outermost blue curve); the relaxation time was computed using the exact method described in the appendix. As can be seen,  $\Omega_0$

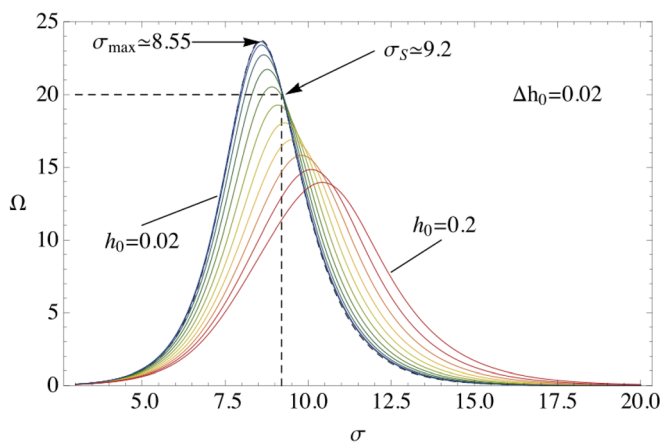


FIG. 1. Efficiency  $\Omega = A/h_0^2$  vs.  $\sigma = K_V/k_B T$  for different values of the reduced applied field amplitude ( $h_0$ ), ranging from 0.02 to 0.2 in steps of 0.02. The frequency is fixed at  $f\tau_0 = 10^{-4}$  (or  $f \approx 100$  kHz for  $\tau_0 \sim 10^{-9}$  s). The linear response efficiency  $\Omega_0$  [Eq. (4)] is shown in dashed. Also shown are the two characteristic values of  $\sigma$ ; namely, the linear response maxima  $\sigma_{\max} \approx 8.5$  and the zero-slope threshold  $\sigma_s \approx 9.2$ , which separate the regions of increasing and decreasing slope as  $\Omega$  departs from the linear regime.

shows a narrow peak with a maximum whose position ( $\sigma_{\max}$ ) is determined by the relation

$$\omega\tau = 1. \quad (5)$$

Finally, it is important to emphasize that Eq. (3) does not represent the efficiency of the material in eliminating tumorous cells *per se* (which is simply given by  $A$  or the SAR), but only a measure of the input/output gain.

Notwithstanding its interesting physical interpretation, the fact that in the linear regime  $\Omega_0$  is independent of  $H_0$  makes the efficiency an extremely convenient quantity: graphing  $\Omega$  vs.  $H_0$  should yield a horizontal line so that any deviations may be readily interpreted as stemming from the departure to the non-linear regime. We note in passing that, since  $A$  must eventually saturate, we necessarily have that  $\Omega(H_0) \rightarrow 0$  when  $H_0 \rightarrow \infty$ ; that is, if  $\Omega$  ever increases, it must eventually reach a maximum. In this paper we employ numerical simulations to probe the behavior of  $\Omega(H_0)$  in detail. However, before we proceed, we show how it is possible to obtain an approximate answer by a remarkably simple heuristic argument, as follows.

The value  $\sigma_{\max}$  determined by Eq. (5) coincides with the condition that the measurement time, here one period of  $H(t)$ , match the relaxation time. Whence,  $\sigma < \sigma_{\max}$  characterizes a low barrier region where the spins may precess nearly unimpeded. Conversely,  $\sigma > \sigma_{\max}$  corresponds to a high barrier regime in which the spins tend to be blocked and may, at most, precess close to the potential wells. We therefore reach the following important conclusion. If  $\sigma < \sigma_{\max}$ , small fields are already capable of promoting spin reversals, and thence the efficiency should *decrease* as  $H_0$  increases. On the other hand, if  $\sigma > \sigma_{\max}$ , the spins will be essentially blocked, requiring

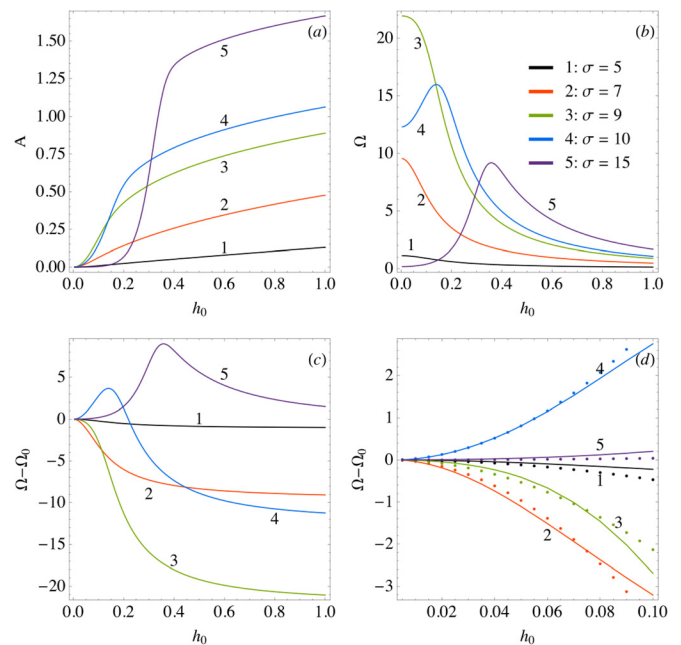


FIG. 2. Area and efficiency vs. the reduced applied field amplitude ( $h_0$ ) for different values of  $\sigma$ , with fixed  $f\tau_0 = 10^{-4}$ . (a) Hysteresis loop area ( $A$ ); (b) efficiency ( $\Omega = A/h_0^2$ ); (c) difference between  $\Omega$  and the linear response efficiency  $\Omega_0$  [Eq. (4)]; and (d) magnification of image (c) for small fields. Points were computed to Eqs. (7) and (8).

larger fields to promote efficient reversals; consequently,  $\Omega$  should *increase* with increasing field.

This analysis is correct, except for the fact that the transition value is actually greater than  $\sigma_{\max}$  by a small factor. We refer to this new value as the zero-slope threshold,  $\sigma_s$ . The reason for this discrepancy may be understood qualitatively by considering that the presence of the field alters the energy landscape of the particle and, as is well known, lowers the relaxation time. Thus, for condition (5) to be met, a larger value of  $\sigma$  is required to counterbalance the presence of the external field. We also note that, as asserted from our simulations, this shift is independent of frequency and has the value  $\sigma_s - \sigma_{\max} \simeq 0.65$  (cf., the upcoming Fig. 1).

Thus, although we will not present any experimental data in this paper, it is clear from the above arguments that the efficiency concept can be used to identify if a given nanoparticle system is in the high or low barrier regime. Such information, in turn, may be employed to delineate strategies to enhance the hyperthermia properties of the material, thus being clearly of considerable importance.

### III. NÉEL-BROWN THEORY

We now turn to the Néel-Brown theory, which may be used to compute the SAR in any condition desired and thence validate the arguments of the preceding section. The starting point for our simulations is the stochastic Landau-Lifshitz equation<sup>29</sup> for the magnetization  $\mathbf{M}(t)$  of a single-domain particle,

$$\dot{\mathbf{M}} = -\gamma \mathbf{M} \times \mathbf{H}_e - (\gamma\alpha/M_s) \mathbf{M} \times (\mathbf{M} \times \mathbf{H}_e), \quad (6)$$

where  $\alpha$  is the damping constant,  $M_s$  is the saturation magnetization,  $\gamma = \gamma_0/(1 + \alpha^2)$  and  $\gamma_0$  is the gyromagnetic factor of the electron. Here  $\mathbf{H}_e$  is the effective field which comprises, besides the external field, a term describing the uniaxial anisotropy and a random thermal field to account for the thermal fluctuations.

We restrict the discussion to the situation where the external field is parallel to the anisotropy easy axis.<sup>24,25</sup> Albeit not realistic, this condition is known to give an adequate qualitative description of the system's response and is advantageous for its low computational cost, thus enabling a more detailed investigation. Moreover, and perhaps most importantly, it enables us to reduce to only three the number of parameters required to fully describe the system:  $h_0 = H_0/H_A$ , where  $H_A = 2K/M_s$ ;  $\sigma = K_V/k_B T$ ; and  $f\tau_0$ , where  $\tau_0 = (\gamma H_A)^{-1}$ . Note that  $\tau_0$  is now the only quantity where the damping appears explicitly. Accordingly, definition (3) is now modified to read  $\Omega = A/h_0^2$ . Real values for  $A$  and  $\Omega$  are obtained by multiplying the quantities presented here by  $M_s H_A$  and  $M_s/H_A$ , respectively.

Details of the computational procedure are given in the Appendix. The solution method we employ consists of transforming the stochastic differential equation (6) into a system of ordinary differential equations for the averages (statistical moments) of the magnetization.<sup>17,19,25,26,30</sup> This approach is not only extremely efficient computationally but is also numerically exact, in the sense that it does not require statistical averages over the stochastic trajectories, as is needed in the

direct solution of Eq. (6).<sup>40</sup> We also note that it can be easily extended to the more general situation where the field is not parallel to the anisotropy axis, as discussed in detail in Ref. 17.

## IV. RESULTS AND DISCUSSION

### A. Numerical results

Before we proceed we call attention to the weak dependence of  $A$  and  $\Omega$  on the frequency. Indeed, if we take  $\tau \simeq \tau_0 e^\sigma$  then Eq. (5) implies  $\sigma \simeq -\log(\omega\tau_0)$  so that increasing (decreasing) the frequency will only shift, logarithmically, the peak in  $\Omega_0$  to lower (higher) values of  $\sigma$ . Accordingly, except for Fig. 4, we fix throughout this paper  $f\tau_0 = 10^{-4}$ . This is motivated by the fact that taking the common experimental value  $\tau_0 \sim 10^{-9}$ s yields  $f \sim 100$  kHz, which agrees with frequencies usually employed in hyperthermia experiments.<sup>3,10,35,41</sup>

In Fig. 1 we present results for  $\Omega$  vs.  $\sigma$ . First and foremost, it is possible to see that the curve for  $h_0 = 0.02$  practically coincides with the linear response efficiency (dashed line). As the field increases,  $\Omega$  gradually deviates from  $\Omega_0$ , being simultaneously broadened and shifted to the right. The chosen value of  $f\tau_0$  results in  $\sigma_{\max} \simeq 8.55$  and  $\sigma_s \simeq 9.2$ . The former agrees with condition (5) using the exact relaxation time, and the latter was determined by the fitting procedure described in Sec. B. From the figure it is clear that for  $\sigma < \sigma_s$ , all curves lie below  $\Omega_0$ , while the opposite occurs for  $\sigma > \sigma_s$ .

The dependence with  $h_0$  is presented in Fig. 2 for both  $A$  and  $\Omega$ . As mentioned, the area (Fig. 2(a)) always increases monotonically with  $h_0$ . At low  $\sigma$  the increase is rather small and so is the value at saturation. At the other extreme, at high  $\sigma$ ,  $A$  remains close to zero up to a certain field, above which it rises quickly, crossing the other curves and finally saturating at large values. The efficiency, plotted in Fig. 2(b), enables for a much more transparent interpretation. First note that  $\Omega$  starts at  $\Omega_0$  (cf., Fig. 1), which is large for  $\sigma \sim \sigma_s$  and negligible otherwise. Furthermore, it is now quite clear that curves for  $\sigma < \sigma_s$  always have a negative slope and decrease monotonically towards zero. The converse is true for  $\sigma > \sigma_s$ :  $\Omega$  starts with a positive slope, reaches a maxima, and then falls towards zero. The higher the value of  $\sigma$ , the larger is the field where the maxima is reached.

In Fig. 3 we condense the results of the previous figures by showing the behavior of  $A$  and  $\Omega$  in the form of a density

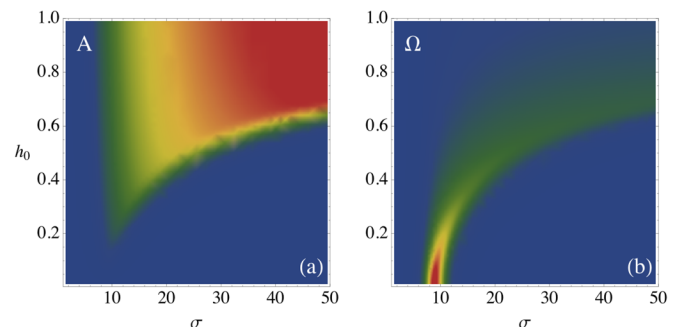


FIG. 3. (a) Area and (b) efficiency vs.  $(\sigma, h_0)$  with fixed  $f\tau_0 = 10^{-4}$ . The color scale is in arbitrary units, with blue and red denoting small and large quantities, respectively. The resolution is  $\Delta\sigma = 0.25$  and  $\Delta h_0 = 0.005$ .

plot in the  $(h, \sigma)$  plane, where blue and red denote small and large quantities, respectively. As for the area, two points are worth noting. First, when  $\sigma \gg \sigma_s$ , one observes an abrupt change as the field increases. This marks the threshold field, above which the promotion of spins over the anisotropy barrier becomes possible.<sup>1</sup> Second, at the opposite extreme ( $\sigma \ll \sigma_s$ ), even at high fields such as  $h_0 = 1$  (i.e.,  $H_0 = H_A$ , a quite high value), the area is still significantly small. This illustrates the fact that simply increasing the field amplitude irrespective of the properties of the material is clearly not a fruitful approach. As for the efficiency (Fig. 3(b)), one sees that its overall maxima in the  $(h, \sigma)$  plane occurs precisely at the linear response value  $\sigma_{\max} \simeq 8.5$  (cf., Eq. (5)). Then, on increasing  $h_0$ , the function  $\Omega(\sigma)$  is simultaneously broadened and shifted to higher values of  $\sigma$ , as is also seen in Fig. 1.

## B. Series expansion of the efficiency

Previous attempts to quantify the field dependence of  $A$  (or equivalently the SAR) have customarily resorted to numerical fits of exponents in a power law,  $A \propto H_0^n$ . While such a procedure has been extremely relevant in understanding the magnetic properties of a variety of magnetic materials,<sup>27</sup> this is not true for hysteresis loops in single-domain nanoparticles. Indeed, this approach, which has already been vehemently criticized,<sup>1</sup> yields results which are quite arbitrary in the sense that practically no physical information may be extracted from them. On the other hand, we now show how it is possible to gain additional insight on the initial deviations from linearity by considering the area as a formal series expansion in powers of  $H_0$ , with coefficients that depend on  $\sigma$  and  $\omega$ . In this sense, Eq. (1) may be regarded as the smallest non-vanishing term. Clearly, this springs from expanding  $M$  in powers of  $H_0$ . For systems in thermal equilibrium, due to symmetry arguments, the expansion will only contain odd powers of  $H_0$ . Then the area, being the product of  $M$  and  $H$ , will contain only even powers, the next term being proportional to  $H_0^4$ . Notwithstanding the fact that the present system is obviously not in thermal equilibrium, we have found this approach to be both simple and effective. Whence, we write

$$\Omega \simeq \Omega_0 + c_2(\sigma, \omega)h_0^2. \quad (7)$$

The quantity  $\Delta\Omega = \Omega - \Omega_0$  is plotted in Figs. 2(c) and 2(d), the latter being a magnification of the former at small fields. In Fig. 4(a) we present the fitted values of  $c_2(\sigma, \omega)$  for  $h_0 < 0.1$

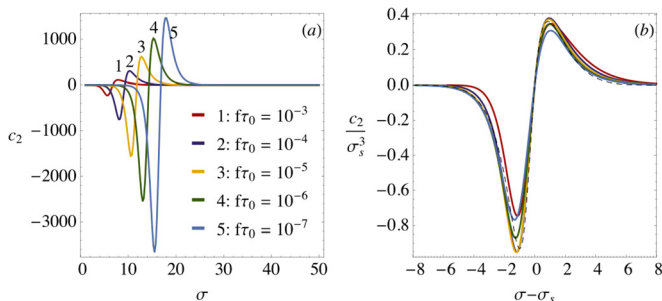


FIG. 4. (a) Next term,  $c_2(\sigma, \omega)$ , in the power series expansion of  $\Omega$  [Eq. (7)], fitted from the initial values of  $\Omega(h_0)$  up to  $h_0 \simeq 0.1$ . (b) Plot of  $c_2/\sigma_s^3$  vs.  $\sigma - \sigma_s$  showing that all curves approximately overlap. The approximate expression given by Eq. (8) is presented in dashed.

at five different frequencies. The following conclusions may be drawn from this analysis:

- $c_2 = 0$  at  $\sigma_s$  (by definition). It is reasonable to expect that the entire frequency dependence is contained within  $\sigma_s$  and so we write  $c_2(\sigma, \omega) = c_2(\sigma, \sigma_s)$ .
- $c_2 \geq 0$  for  $\sigma \geq \sigma_s$ , reflecting the fact that  $\Delta\Omega$  is positive for  $\sigma > \sigma_s$  and negative otherwise.
- $c_2 \rightarrow 0$  at  $\sigma \sim 0$  and  $\sigma \gg \sigma_s$ . As expected, at small  $h_0$  the response for the low and high barrier regimes are nearly equivalent. However, note that albeit small, the slope of  $\Delta\Omega$  (which is simply  $2c_2$ ) has indeed opposite signs in both regimes [cf., Fig. 2(d) for  $\sigma = 5$  and  $\sigma = 15$ ].
- $c_2$  is not symmetrical about  $\sigma_s$ , being much larger for  $\sigma < \sigma_s$ . That is, the efficiency falls much more rapidly for  $\sigma < \sigma_s$  than it rises for  $\sigma > \sigma_s$ .
- While the functional dependence of  $c_2$  is clearly seen to depend only on  $\sigma - \sigma_s$ , the overall height is different for each frequency. We have found that this scales as  $\sim \sigma_s^3$ .

A thorough attempt to obtain elaborate analytical expressions for  $c_2(\sigma, \omega)$  is beyond the scope of this paper, especially given the non-linearity of the problem which would undoubtedly yield utterly complicated results, if any. However, it is interesting to note that, as shown in Fig. 4(b), all curves can be made to approximately overlap by plotting  $c_2/\sigma_s^3$  vs.  $\sigma - \sigma_s$ . Moreover, they are quite well described by the function

$$\frac{c_2(\sigma, \sigma_s)}{\sigma_s^3} = \frac{4x/3}{1 + (x + 1/2)^2} e^{-(x/3)^2}, \quad (8)$$

where  $x = \sigma - \sigma_s$ . This result was derived heuristically by choosing a function which satisfied all the properties of  $c_2$  just listed. The series in Eq. (7), together with Eq. (8) is plotted in Fig. 2(d), where, as can be seen, the agreement is indeed satisfactory up to  $h_0 = 0.1$ . We emphasize that the importance of this discussion lies on the properties that  $c_2$  must satisfy and not on Eq. (8) or other similar functions. Hopefully, these properties may serve as useful guidelines for theoreticians developing realistic non-linear models.

## C. Discussion

All results presented thus far are equally valid for the SAR, which is almost always measured at a fixed frequency. Thus, we have shown that plotting the  $SAR/H_0^2$  vs.  $H_0$  provides an interesting way of analyzing experimental data. From the slope of  $\Omega$  it is possible to determine whether the particles are in a low or high barrier regime. Moreover, while a measure of the slope may not give a quantitative estimate of  $\sigma$ —due to the inherent complexities of experimental systems—this may be achieved by comparing different samples.

For completeness, let us consider a comparative example between two given samples, described by (say) curves 4 and 5 in Fig. 2. If one has access only to a limited field amplitude (e.g.,  $h_0 < 0.1$ ), an analysis of the area yields no information about curve 5 [Fig. 2(a)]. Conversely, the efficiency may indicate a small increasing slope which enables

one to assert that curve 5 is far into the high barrier regime and not the opposite [Fig. 2(d)]. Moreover, if both samples have roughly the same mass and saturation magnetization, the initial efficiency immediately shows that curve 4 will also be in the high barrier regime, but with a value of  $\sigma$  smaller than that of curve 5.

This comparison permits one to rank several samples according to different (qualitative) values of  $\sigma$ , without any explicit reference to neither anisotropy nor volume nor packing fraction. This is of particular importance for a variety of reasons. First, the actual value of  $\sigma$  is usually smeared by the size distribution and simultaneously shifted due to particle-particle interactions. Moreover, the region in the  $\sigma$  axis where  $\Omega$  is appreciably different from zero depends not only on  $f$  but also on  $\tau_0$ , which is rarely known to any satisfactory accuracy. Notwithstanding, this approach is impermeable to these difficulties since a simple relative ranking of the particles already yields considerable information.

This analysis also suggests a way to manage magnetic materials in order to enhance its hyperthermia properties. This follows since  $\sigma \propto Kv$  so that a change in volume or in anisotropy is entirely equivalent (at least within the single-domain approximation). For instance, if one discovers that for a given particle size the system is in the low (high) barrier regime, one could improve the dissipation by increasing (decreasing) the magnetic anisotropy value. Indeed, the fact that  $\Omega(\sigma)$  is usually a narrowly peaked function further corroborates the necessity of such fine tuning. The importance of optimum magnetic anisotropies has already been discussed by several authors<sup>1,34</sup> and is also endorsed by other aspects of the application. For instance, although not commonly discussed, the feasibility of producing highly-stable colloids is greatly enhanced by using lower particle sizes (probably in the 10 nm range). The same is true for embolization issues, as follows from its lower agglomerate dimensions.<sup>42</sup> Thus, from the perspectives of both the heating power and colloidal stability, the ability to tune the magnetic anisotropy is seen as being paramount to the success of magnetic hyperthermia. Fortunately, in ferrites, this can be performed with great flexibility either by modifying the cation distribution in the spinel structure or through atom-substitution.<sup>2,3,43,44</sup>

The results in Fig. 2(a) are quite similar to experiments recently reported by Bordelon *et al.*<sup>35</sup> using commercial ferrite samples (cf., Fig. 5). A rough estimate considering the magnetite bulk anisotropy ( $K \simeq 2.3 \times 10^5 \text{ erg/cm}^3$ ) yields  $\sigma$  in the ranges of 0.2–3, 3–5, and 10–23, for the Feridex (4–10 nm), nanomag-D-sprio (10–12 nm), and BNF-starch (15–20 nm) samples, respectively, i.e., very similar to the values presented in Fig. 2. Thus, their results may be readily interpreted within the present scope as arising from different values of  $\sigma$ . Similar arguments apply to the results in Fig. 5(a) of Ref. 3. In this case, it is worth pointing out that the differences are brought about not only by the changes in the size of the particles but also by those in their anisotropies, stemming from the different cation distribution/substitution of the ferrites studied. Finally, we note that in both cases the limited number of experimental points also endorses the use of the efficiency: interpreting an increasing

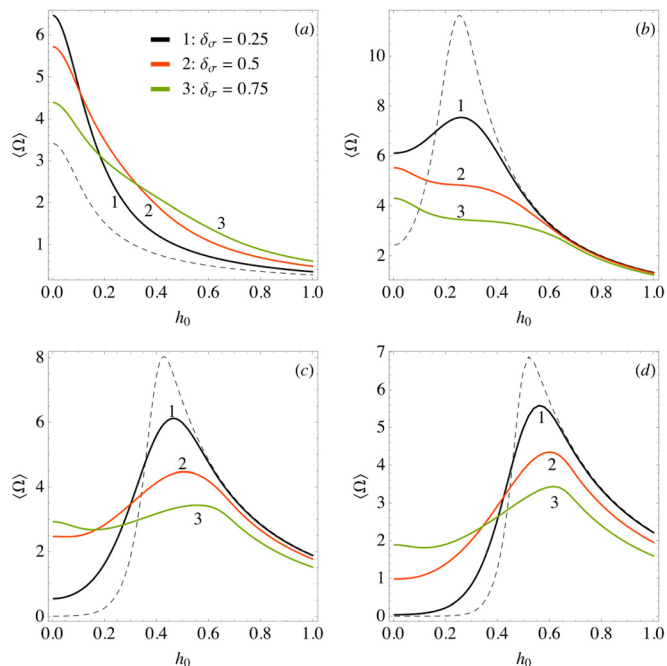


FIG. 5. Poli-disperse efficiency  $\langle \Omega \rangle$  vs.  $h_0$  for three values of the dispersion parameter  $\delta_\sigma$ . Mono-disperse curves are shown in dashed. (a)  $\sigma_0 = 6$ , (b)  $\sigma_0 = 12$ , (c)  $\sigma_0 = 18$ , and (d)  $\sigma_0 = 24$ .

or decreasing trend starting from a horizontal line is far simpler than interpreting a rapidly increasing function.

Our numerical simulations clearly show that within the present (several) approximations, the initial slope of the efficiency is directly related to the height of the energy barrier. It is not possible for us to claim that this will remain true in more realistic situations. We nonetheless do have reasons to believe so. First, several tests for randomly oriented ensembles (not shown) indicate that, as we expect, taking the field as parallel to the anisotropy axis does not yield incorrect predictions. More importantly however, is the fact that the simple heuristic arguments given in Sec. II agree quite well with the numerical simulations. These arguments were based solely on the concept of an energy barrier, which is a very general assumption that is true for any system. Therefore, such an agreement serves as powerful evidence that the scope of applicability of the present results is indeed much wider. Conversely, the effect of inter particle interactions is not entirely clear and we are unable to make any definitive judgements: the long-range nature of the dipolar interaction renders this as a many-body problem, the properties of which remain a subject under discussion. We also note in passing that simulations including dipolar interaction are much more expensive computationally, given that the methods described in the Appendix are not applicable; the only alternative is the direct solution of the stochastic differential Eq. (6), which involves the use of a large quantity of random numbers. Finally, there remains the problem of poli-dispersivity, which, as we now show, also does not invalidate our results.

## V. INFLUENCE OF THE SIZE DISPERSION

We briefly consider the effect that a poli-disperse sample has on the efficiency. For definiteness, we assume

spherical particles with diameters distributed according to a log-normal distribution. We use the notation  $x \approx \mathcal{L}(x_0, \delta_x)$  to denote that the random variable  $x$  is distributed according to a log-normal distribution with location parameter  $x_0$  and dispersion parameter  $\delta_x$ . The probability density function is

$$p(x) = \frac{1}{\sqrt{2\pi x \delta_x}} \exp \left[ -\frac{(\log(x/x_0))^2}{2\delta_x^2} \right]. \quad (9)$$

A useful and sometimes unexplored property of the log-normal distribution is as follows: if  $y = ax^n$  and  $x \approx \mathcal{L}(x_0, \delta_x)$ , then  $y \approx \mathcal{L}(y_0, n\delta_x)$ , where  $y_0 = ax_0^n$ . In other words,  $y$  is also distributed according to a log-normal distribution, with a dispersion parameter that is  $n$  times larger than that of  $x$ . This relation follows immediately from the definition  $p(y) dy = p(x) dx$ .

Thus, if a sample has a diameter distribution of the form  $D \approx \mathcal{L}(D_0, \delta_D)$ , then  $\sigma \approx \mathcal{L}(\sigma_0, \delta_\sigma)$ , where  $\sigma_0 = K v_0 / k_B T = \pi K D_0^3 / (6 k_B T)$  and  $\delta_\sigma = 3\delta_D$ . Usual size distributions reported in the literature<sup>45,46</sup> have  $\delta_\sigma \lesssim 0.25$  yielding  $\delta_\sigma \lesssim 0.75$ .

Numerical simulations for poly-disperse samples are computed by taking the expectation value of the mono-disperse results with respect to Eq. (9). In Fig. 5 we present results for the average efficiency ( $\langle \Omega \rangle$ ) vs.  $h_0$ , for different values of  $\sigma_0$  and  $\delta_\sigma$ , once again fixing  $f\tau_0 = 10^{-4}$ . As one might expect, the response for poly-disperse systems is quite different. The key point is that for each value of  $h_0$  (and  $\omega$ ), the original function  $\Omega(\sigma)$  is appreciably different from zero only over a narrow range of  $\sigma$ , which is also asymmetrical with respect to its maximum. The same is obviously true for  $p(\sigma)$ : it is both narrow and asymmetrical. Thus, on convolving  $\Omega(\sigma)$  with  $p(\sigma)$ , only those regions where there is considerable overlap will give a response that is appreciably different from zero.

In Fig. 5(a), where  $\sigma = 6$ , it is possible to see that increasing  $\delta_\sigma$  increases the overall value of  $\langle \Omega \rangle$ . Clearly, as shown in Fig. 1, the response for  $\sigma = 6$  itself is almost negligible so that, on increasing the dispersion, higher values of  $\sigma$  start to contribute more substantially. The situation reverses for  $\sigma = 12$ , where the statistical importance of those values of  $\sigma$  which are much smaller than  $\sigma_s$  are seen to gradually increase with  $\delta_\sigma$ , whereas their contribution to  $\Omega(\sigma)$  remains quite small. It is also interesting to note that due to the complex dependence on  $h_0$ , the efficiency may initially decrease but then increase, as illustrated by curve 3 in Fig. 5(c).

Even though the size distribution smears the result, in the sense of making it less clear to discern between the high and low barrier regimes, it remains possible to rank different samples in precisely the same way. Thus, the arguments of the preceding section remain entirely valid in this case. As for the ranking, one may either use  $\sigma_0$ , which is the median of Eq. (9), or the mean, which is  $\bar{\sigma} = \sigma_0 e^{\delta_\sigma^2/2} = \sigma_0 e^{9\delta_D^2/2}$  (the latter is larger than the former by a factor of  $\sim 30\%$  when  $\delta_\sigma = 0.75$ ).

## VI. CONCLUSIONS

In this paper we analyzed the properties of magnetic nanoparticles intended for magnetic hyperthermia applications from the view point of a new parameter, referred to as the

energy transfer efficiency. This is computed simply as the ratio between the power (or energy) loss and the square of the field amplitude:  $(\text{SAR}/H_0^2)$ . Besides having an interesting physical interpretation, we have shown that this approach enables a much richer analysis of the experimental data, giving information on the behavior of the system as it departs from the low field linear regime. From a graph of the efficiency vs. the field amplitude, we have found that a simple qualitative analysis is capable of yielding significant information about the anisotropy energy barrier distribution. As is now being realized by the community, the anisotropy is paramount in enhancing the heating capabilities of nanoparticles for magnetic hyperthermia. Moreover, exploiting its intimate relation with the field amplitude is now seen as the most promising route towards sizable advances in this important application.

One final important point should be clarified. The present paper does not suggest that the efficiency should replace the SAR. On the contrary, we have shown that they are in fact complementary and may be presented together. The SAR, on one hand, yields the system's heating capabilities, and the efficiency, on the other hand, points to whether the system lies in the low or high barrier regime, thence providing guidelines to further optimize the SAR.

## ACKNOWLEDGMENTS

The authors acknowledge the Brazilian funding agencies CNPq, CAPES, FINEP, FAPEG, FAPESP, and FUNAPE.

## APPENDIX: SOLUTION METHODS

Under the assumptions discussed in Sec. III that the field is parallel to the anisotropy axis (here taken as the z-axis), the quantity of interest is  $\langle m_z \rangle$ , where  $\mathbf{m} = \mathbf{M}/M_s$ . By averaging Eq. (6) using the methods of stochastic calculus,<sup>30</sup> the non-linearity of the equations force all statistical moments to be entangled; in other words, the differential equation for the time evolution of  $\langle m_z \rangle$  will depend, for instance, on  $\langle m_z^2 \rangle$ . The results may be expressed, however, as a system of coupled ordinary differential equations, also referred to as a hierarchy of differential recurrence relations. We use spherical coordinates with  $m_z = \cos\theta$  and expand these moments in terms of Legendre polynomials,  $P_n(x)$  (i.e.,  $\langle m_z \rangle = \langle P_1(\cos\theta) \rangle$ ). Let  $p_n = \langle P_n(\cos\theta) \rangle$ . Then, by the methods described in Refs. 17, 19, 25, and 26, we obtain

$$\begin{aligned} \tau_0 \dot{p}_n - \left[ \frac{n(n+1)}{(2n-1)(2n+3)} - \frac{n(n+1)}{2\sigma} \right] p_n &= \frac{n(n^2-1)}{4n^2-1} p_{n-2} \\ &- \frac{n(n+1)(n+2)}{(2n+1)(2n+3)} p_{n+2} + h \frac{n(n+1)}{2n+1} (p_{n-1} - p_{n+1}), \end{aligned} \quad (\text{A1})$$

where  $h = h_0 \cos\omega t$  and  $n = 1, 2, \dots$

Let us then define the column vector  $\mathbb{P} = [p_1, p_2, \dots, p_N]^T$ , where  $N \sim 200$  is taken large enough to ensure convergence. Then, by collecting the terms in Eq. (A1) we may transform it in a system of first order ordinary linear differential equations

$$\dot{\mathbf{P}} = \mathcal{F}\mathbf{P} + \mathbf{U}, \quad (\text{A2})$$

where  $\mathcal{F}$  is an  $N \times N$  matrix and  $\mathbf{U}$  is a column vector of length  $N$ , both of which depend on time implicitly through  $h(t)$ .

The hysteresis loops are computed integrating the system of Eq. (2) until transient effects are eliminated, thus yielding a stationary solution. The matrix  $\mathcal{F}$ —which is also the Jacobian of the system—is tightly banded, a property which if cleverly explored yields considerable gains in computational speed. We employed the SUNDIALS library,<sup>47</sup> which enabled computation times  $\lesssim 1$ s for each loop. We note that for practical purposes transients are entirely unimportant for magnetic hyperthermia for, albeit being able to persist for over 100 periods of the external field, when one considers the high frequencies involved, this only accounts for micro-seconds which are negligible compared to the usual measurement times that are of the order of several seconds.

Further details of this method are described in Refs. 17 and 25. We refer the reader to Refs. 18, 19, and 24 for a different solution method stemming from the same system of equations or Refs. 1 and 20 for a different approach based on transition state theory.

Finally, we note that the exact relaxation time [cf., Eq. (2)] may be easily computed from the matrix  $\mathcal{F}$  by setting  $h = 0$ . In this case the difference between the relaxation time and the *smallest non-vanishing eigenvalue* of  $\mathcal{F}$ ,  $\lambda_1$ , is negligible. This yields an incredibly efficient way of computing  $\tau$  since, due the strong sparseness of  $\mathcal{F}$  (in this case it actually becomes tri-diagonal), Arnoldi's iterative method<sup>48</sup> may be employed to calculate only  $\lambda_1$ . In fact, it is interesting to note that this approach is much faster than using the exact solution for  $\lambda_1$ , which is written in terms of sums of hypergeometric functions<sup>31</sup> that are usually computationally expensive.

- <sup>1</sup>J. Carrey, B. Mehdaoui, and M. Respaud, *J. Appl. Phys.* **109**, 083921 (2011).
- <sup>2</sup>M. Veverka, Z. Jiráček, O. Kaman, K. Knížek, M. Maryško, E. Pollert, K. Závěta, A. Lančok, M. Dlouhá, and S. Vratislav, *Nanotechnology* **22**, 345701 (2011).
- <sup>3</sup>I. Sharifi, H. Shokrollahi, and S. Amiri, *J. Magn. Magn. Mater.* **324**, 903 (2012).
- <sup>4</sup>A. Pankhurst, N. K. T. Thanh, S. K. Jones, and J. Dobson, *J. Phys. D: Appl. Phys.* **42**, 224001 (2009).
- <sup>5</sup>A. Jordan, R. Scholz, P. Wust, H. Fahling, J. Krause, W. Włodarczyk, B. Sander, T. Vogl, and R. Feliz, *Int. J. Hyperthermia* **13**, 587 (1997).
- <sup>6</sup>A. Ito, H. Honda, and T. Kobayashi, *Cancer Immunol. Immunother.* **55**, 320 (2006).
- <sup>7</sup>J. Giri, P. Pradhan, T. Sriharsha, and D. Bahadur, *J. Appl. Phys.* **97**, 10Q916 (2005).
- <sup>8</sup>L. Dennis, A. J. Jackson, J. A. Borchers, P. J. Hoopes, R. Strawbridge, A. R. Foreman, J. van Lierop, C. Grüttner, and R. Ivkov, *Nanotechnology* **20**, 395103 (2009).
- <sup>9</sup>H. A. Guedes, N. Sadeghiani, D. L. G. Peixoto, J. P. Coelho, L. S. Barbosa, R. B. Azevedo, S. Kückelhaus, M. D. F. Da Silva, P. C. Morais, and Z. G. M. Lacava, *J. Magn. Magn. Mater.* **293**, 283 (2005).

- <sup>10</sup>W. Andrä, C. G. D'Ambly, R. Hergt, I. Hilger, and W. A. Kaiser, *Int. J. Hyperthermia* **24**, 467 (2008).
- <sup>11</sup>S. Eggeman, S. A. Majetich, D. Farrell, and Q. A. Pankhurst, *IEEE Trans. Magn.* **43**, 2451 (2007).
- <sup>12</sup>W. Andrä, C. G. D'Ambly, R. Hergt, I. Hilger, and W. A. Kaiser, *J. Magn. Magn. Mater.* **194**, 197 (1999).
- <sup>13</sup>E. Sosnovik, M. Nahrendorf, and R. Weissleder, *Circulation* **115**, 2076 (2007).
- <sup>14</sup>H. Chung, A. Hoffmann, K. Guslienko, S. D. Bader, C. Liu, B. Kay, L. Makowski, and L. Chen, *J. Appl. Phys.* **97**, 10R101 (2005).
- <sup>15</sup>T. Coffey, D. S. F. Crothers, Y. P. Kalmykov, and S. V. Titov, *Phys. Rev. B* **64**, 012411 (2001).
- <sup>16</sup>H. Ebert, S. Mankovsky, D. Ködderitzsch, and P. J. Kelly, *Phys. Rev. Lett.* **107**, 066603 (2011).
- <sup>17</sup>G. T. Landi, *J. Appl. Phys.* **111**(4), 043901 (2012).
- <sup>18</sup>E. Mrabti, S. V. Titov, P.-M. Déjardin, and Y. P. Kalmykov, *J. Appl. Phys.* **110**, 023901 (2011).
- <sup>19</sup>S. Poperechny, Y. L. Raikher, and V. I. Stepanov, *Phys. Rev. B* **82**, 174423 (2010).
- <sup>20</sup>A. Usov, *J. Appl. Phys.* **107**, 123909 (2010).
- <sup>21</sup>K. Gilchrist, R. Medal, W. D. Shorey, R. C. Hanselman, J. C. Parrott, and C. B. Taylor, *Ann. Surg.* **146**, 596 (1957).
- <sup>22</sup>M. Krishnan, *Trans. Magn.* **46**, 2523 (2010).
- <sup>23</sup>C. Stoner and E. P. Wohlfarth, *IEEE Trans. Magn.* **27**, 3475 (1991).
- <sup>24</sup>P.-M. Déjardin, Yu P. Kalmykov, B. E. Kashevsky, H. El Mrabti, I. S. Poperechny, Y. L. Raikher, and S. V. Titov, *J. Appl. Phys.* **107**, 073914 (2010).
- <sup>25</sup>G. T. Landi and A. D. Santos, *J. Appl. Phys.* **111**, 07D121 (2012).
- <sup>26</sup>G. T. Landi, *J. Magn. Magn. Mater.* **324**, 466 (2012).
- <sup>27</sup>G. Bertotti, *Magnetism*, 1st ed. (Academic, 1998), p. 558.
- <sup>28</sup>B. Mehdaoui, J. Carrey, M. Stadler, A. Cornejo, C. Nayral, F. Delpech, B. Chaudret, and M. Respaud, *Appl. Phys. Lett.* **100**, 052403 (2012).
- <sup>29</sup>F. Brown, *Phys. Rev.* **130**, 1677 (1963).
- <sup>30</sup>T. Coffey, Y. P. Kalmykov, and J. T. Waldron, *Langevin Equation. With Applications to Stochastic Problems in Physics, Chemistry and Electrical Engineering*, 2nd ed. (World Scientific Publishing Co, Pte. Ltd., Singapore, 2004), p. 678.
- <sup>31</sup>T. Coffey, D. S. F. Crothers, Y. P. Kalmykov, E. S. Massawe, and J. T. Waldron, *Phys. Rev. E* **49**, 1869 (1994).
- <sup>32</sup>E. Rosensweig, *J. Magn. Magn. Mater.* **252**, 370 (2002).
- <sup>33</sup>V. Titov, P.-M. Déjardin, H. El Mrabti, and Y. P. Kalmykov, *Phys. Rev. B* **82**, 100413(R) (2010).
- <sup>34</sup>M. Morgan and R. H. Victora, *Appl. Phys. Lett.* **97**, 093705 (2010).
- <sup>35</sup>E. Bordelon, C. Cornejo, C. Gruttner, F. Westphal, T. L. DeWeese, and R. Ivkov, *J. Appl. Phys.* **109**, 124904 (2011).
- <sup>36</sup>K. P. Scaife, *Permittivity* (The English Universities Press, London, 1971).
- <sup>37</sup>F. Bakuzis and P. C. Morais, *J. Magn. Mag. Mater.* **226-230**, 1924 (2001).
- <sup>38</sup>F. Bakuzis, P. C. Morais, and F. Pelegrini, *J. Appl. Phys.* **85**, 7480 (1999).
- <sup>39</sup>F. Bakuzis, P. C. Morais, and F. A. Tourinho, *J. Mag. Reson. Ser. A* **122**, 100 (1996).
- <sup>40</sup>L. García-Palacios and F. J. Lázaro, *Phys. Rev. B* **58**, 14937 (1998).
- <sup>41</sup>M. Johannsen, B. Thiesen, P. Wust, and A. Jordan, *Int. J. Hyperthermia* **26**, 790 (2010).
- <sup>42</sup>L. Castro, G. R. R. Gonçalves, K. S. Neto, P. C. Morais, A. F. Bakuzis, and R. Miotto, *Phys. Rev. E* **78**, 061507 (2008).
- <sup>43</sup>A. M. Brabers, *Phys. Rev. Lett.* **68**, 3113 (1992).
- <sup>44</sup>K. Yosida and M. Tachiki, *Prog. Theor. Phys.* **17**, 331 (1957).
- <sup>45</sup>R. Cintra, F. S. Ferreira, J. L. Santos, Jr., J. C. Campello, L. M. Socolovsky, E. M. Lima, and A. F. Bakuzis, *Nanotechnology* **20**, 045103 (2009).
- <sup>46</sup>T. A. Eloi, J. L. Santos, Jr., P. C. Morais, and A. F. Bakuzis, *Phys. Rev. E* **82**, 021407 (2010).
- <sup>47</sup>C. Hindmarsh, P. N. Brown, K. E. Grant, S. L. Lee, R. Serban, D. E. Shumaker, and C. S. Woodward, *Trans. Math. Software* **31**, 363 (2005).
- <sup>48</sup>E. Arnoldi, *J. Appl. Math.* **9**, 17 (1951).